RESEARCH ARTICLE

Figures and figure supplements

A low Smc flux avoids collisions and facilitates chromosome organization in *Bacillus subtilis*

Anna Anchimiuk *et al*

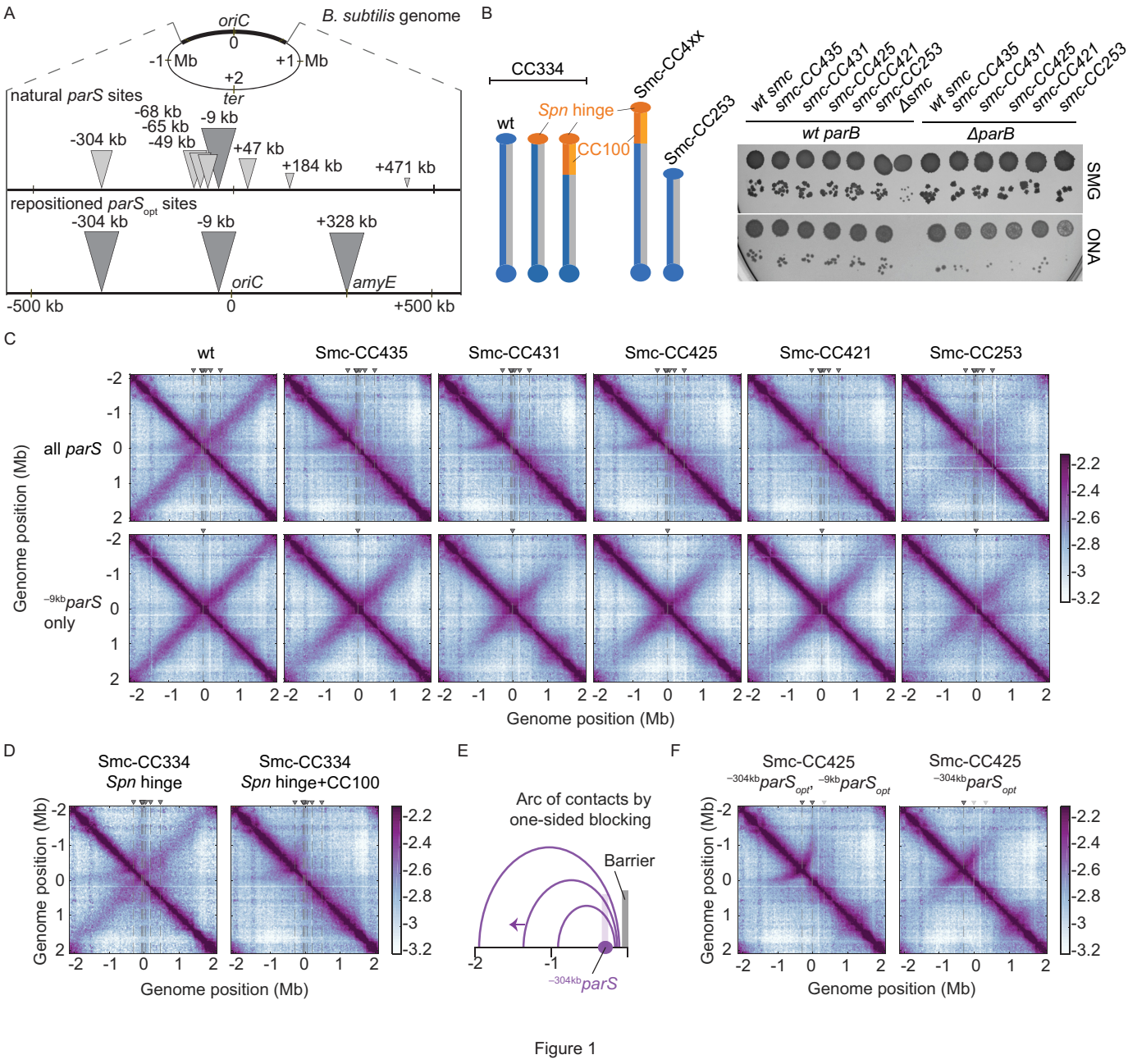

Figure 1

Figure 1. Arm-modified Smc proteins fail to align chromosome arms unless most *parS* sites are removed. (**A**) Upper panel: scheme depicting the natural distribution of *parS* sites on the *B. subtilis* genome. Triangles indicate positions of *parS* sites, size of which is scaled according to ParB occupancy judged by ChIP-seq (***Minnen et al., 2016***). Lower panel: scheme depicting engineered *parS* distribution generated in this study. *parS* sites were either eliminated by mutation or substituted for the $parS_{opt}$ sequence (i.e., the sequence of $^{-9kb}parS$) as needed. For some experiments, an additional site ($^{+328kb}parS_{opt}$) was inserted into the *amyE* locus. (**B**) Left panel: schemes of Smc coiled coil variants investigated in this study: wild-type (CC334), elongated (CC4xx), and shortened (CC253). *Spn* hinge+CC100, *Streptococcus pneumoniae* hinge domain, and 100 amino acids hinge-proximal coiled coil (in orange colors). The coiled coil was shortened or elongated starting from a chimeric protein having the *B. subtilis* Smc hinge domain replaced by the *S. pneumoniae* (*Spn*) Smc hinge domain including an ~100 aa (amino acid) segment of the adjacent coiled coil. Right panel: spotting assay of strains with altered Smc coiled coil in wild-type or sensitized background (Δ*parB*). 9^{-2} and 9^{-5} dilutions were spotted on nutrient-poor (SMG) or nutrient-rich medium (ONA) and imaged after 36 hr and 15 hr, respectively. Note that in the absence of ParB the ParABS system is non-functional and Smc loading is inefficient and untargeted, together putting a strain on chromosome segregation (***Minnen et al., 2016***; ***Wilhelm et al., 2015***). The expression levels of some of these constructs (CC435, CC253) were previously shown to be close to the levels of the wild-type protein by

Figure 1 continued on next page

Figure 1 continued

immunoblotting (***Bürmann et al., 2017***). The levels of Smc-CC425 are evaluated in ***Figure 1—figure supplement 1A***. (**C**) Normalized 3C-seq contact maps obtained from exponentially growing cultures. Top row: strains with wild-type *parS* sites. Bottom row: strains with a single $^{-9kb}parS_{opt}$ (*par-S359*) site. All 3C-seq maps presented in this study are split into 10 kb bins and have the replication origin placed in the middle. The interaction score is in log_{10} scale, the darker the color, the more interactions between given loci (see Materials and methods). (**D**) Normalized 3C-seq contact maps obtained from exponentially growing cultures carrying all the wild-type *parS* sites and wild-type length Smc (Smc-CC344) with either only hinge replaced by the *S. pneumoniae* sequence (*Spn* hinge, left panel) or the hinge together with 100 amino acids of hinge-proximal coiled coil replaced (*Spn* hinge + CC100, right panel). (**E**) Scheme for asymmetric loop extrusion starting at $^{-304kb}parS$ (*parS-334*) due to blockage of translocation towards the replication origin by head-on encounters (with other Smc complexes or RNA polymerase) generating an arc of contacts in the 3C-seq maps. (**F**) Normalized 3C-seq contact maps of elongated Smc (Smc-CC425) carrying $parS_{opt}$ sites at −304 kb and −9 kb (left panel) or $parS_{opt}$ site at −304 kb only (right panel). Triangles above the contact map point to positions of *parS* sites (dark gray triangles indicate active parS sites, light gray triangles for reference are *parS* sites absent in the given experiment).

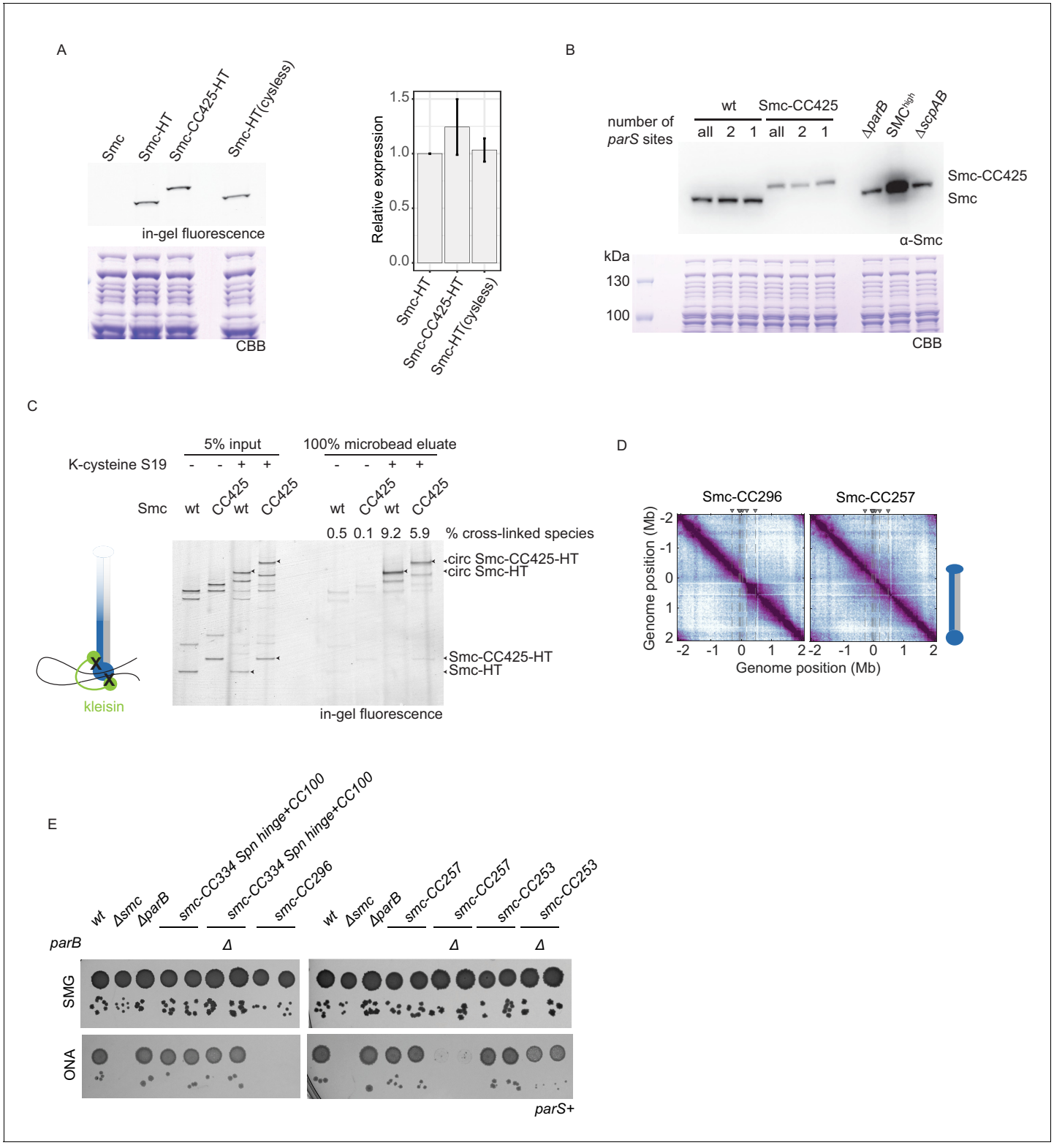

Figure 1—figure supplement 1. Characterization of Smc variants, #1. (**A**) Cellular expression levels of HaloTagged ('HT') versions of wild-type and Smc-CC425. Exemplary SDS-PAGE image obtained by in-gel fluorescence detection (top-left panel) and subsequent Coomassie Brilliant Blue (CBB) staining (bottom-left panel). Quantification of relative expression levels (right panel). Mean and standard deviation obtained from three biological replicates are shown. Smc-HT(cysless) refers to a HT variant in which endogenous cysteines were mutated. (**B**) Immunoblotting using α-Smc (top panel) serum. Protein extracts from wild-type cells and cells with Smc-CC425 (harboring all, two or a single *parS* site) were analyzed. Note that apparently

Figure 1—figure supplement 1 continued on next page

Figure 1—figure supplement 1 continued

reduced levels of Smc-CC425 might be due to poor blotting efficiency of the larger protein or poor recognition of the chimeric protein by the polyclonal Smc antiserum. (**C**) Chromosome co-entrapment assay for HT versions of wild-type and Smc-CC425 with closed Smc-kleisin interface (S152C, S19C, and R1032C in Smc; E52C and H235C in ScpA) and respective control strains lacking one of the two cysteines in ScpA (S19C). Arrowheads indicate the following species: Smc-HT and Smc-CC425-HT as well as the corresponding fully cross-linked, circular species ('circ') of Smc-HT and Smc-CC425-HT. Numbers indicate the relative enrichment of the circular species by chromosome co-entrapment (see Materials and methods) for a representative experiment from three biological replicates. (**D**) Normalized 3C-seq contact maps for strains harboring Smcs with shortened coiled coils that were non-viable (Smc-CC296) or sick on nutrient-rich medium (Smc-CC257). (**E**) Spotting assay of strains with modified Smc coiled coil in wild-type background or sensitized background (Δ*parB*). Prepared as described in ***Figure 1B***. Two independent clones for each tested mutant were spotted. Combining Δ*parB* with Smc-CC296 was unsuccessful. *Spn* hinge + CC100, *Streptococcus pneumoniae* hinge and 100 amino acids of hinge-proximal coiled coil.

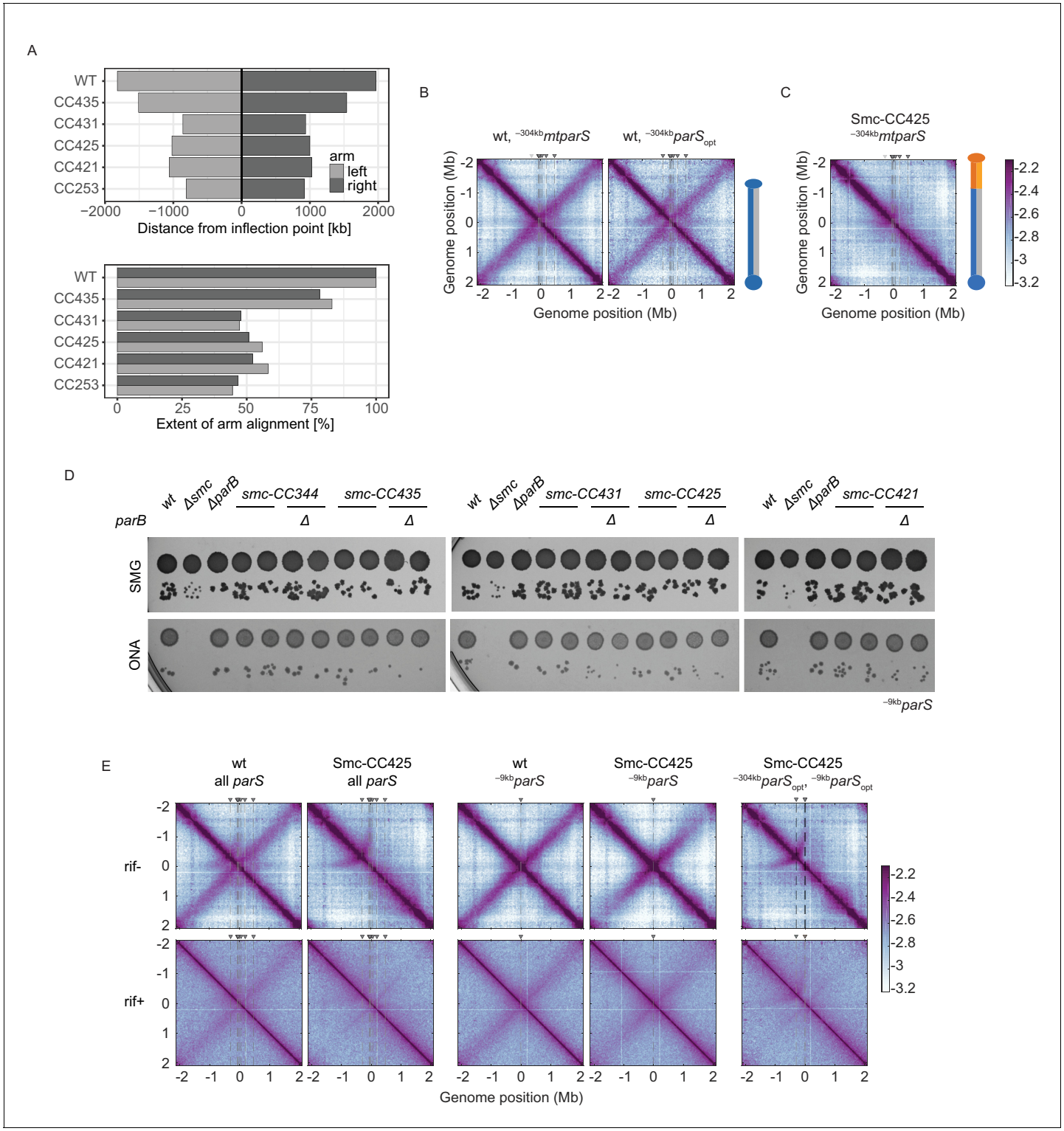

Figure 1—figure supplement 2. Characterization of Smc variants, #2. (**A**) Quantification of the extent of chromosome arm alignment for 3C-seq maps presented in ***Figure 1C***. Plot reporting the extent of juxtaposed arm regions for the right and the left chromosome arm starting from the origin (top panel). Extent of arm alignment relative to wild type (bottom panel). (**B**) Normalized 3C-seq contact maps for strains with mutated $^{-304kb}$*parS* (*parS-334*) (left panel) or its sequence substituted for the $parS_{opt}$ sequence (*parS-359*) (right panel). (**C**) Normalized 3C-seq contact maps for strains with inactivated *parS-334* and Smc-CC425. (**D**) Spotting assay of strains with elongated Smc coiled coil in a genetic background with a single $^{-9kb}parS_{opt}$ (*parS-359*) site with or without *parB*. Prepared as described in ***Figure 1B***. Two clones for each tested mutant were tested. (**E**) RNAP inhibition experiment using

Figure 1—figure supplement 2 continued on next page

Figure 1—figure supplement 2 continued

rifampicin. Normalized 3C-seq contact maps for strains with all, one, or two *parS* sites in wild-type Smc or Smc-CC425 backgrounds (mock treatment controls 'rif-', top panels) ('rif+', bottom panels).

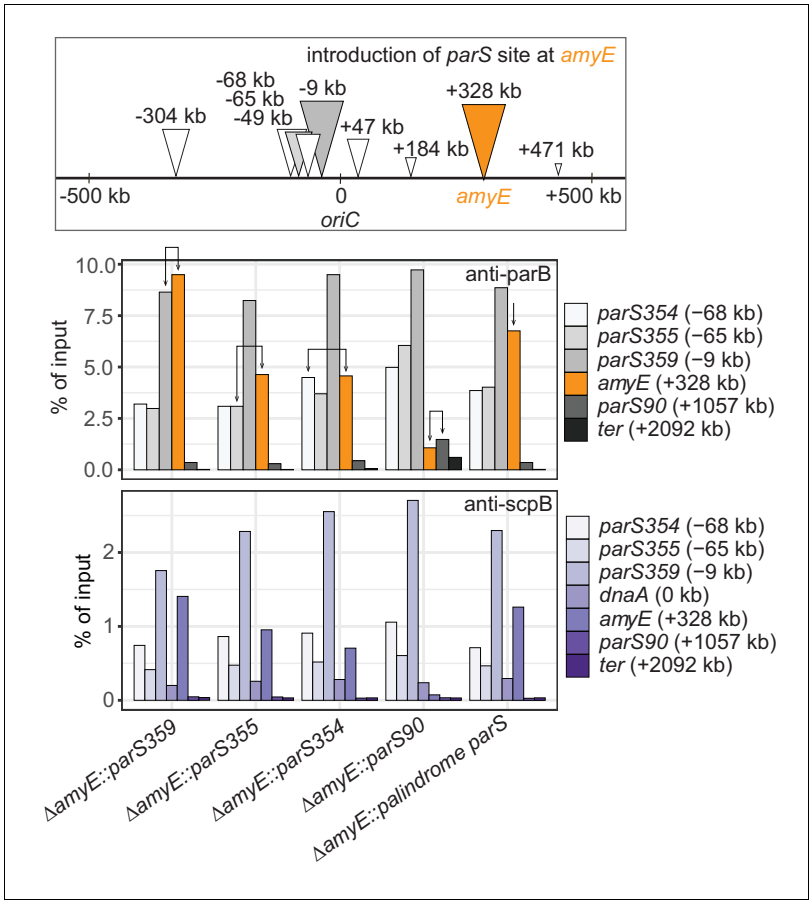

Figure 1—figure supplement 3. Recruitment efficiency of various *parS* sequences. Scheme depicting the experimental setup (top panel): different wild-type *parS* sequences as well as a perfect palindromic *parS* sequence were engineered at *amyE* locus (in orange colors) in an otherwise wild-type background. Chromatin-immunoprecipitation coupled to quantitative PCR (ChIP-qPCR) using α-ParB (middle panel) and α-ScpB serum (bottom panel). Recruitment of ParB to identical *parS* sequences at the endogenous site (gray colors) and engineered site (in orange colors) are indicated with arrows. The enrichment observed by ectopic integration at *amyE* was similar to one seen at the respective endogenous loci, demonstrating that the *parS* sequence determines the efficiency of ParB recruitment largely irrespective of the genomic neighborhood. The strength of natural *parS* sequences appears to decrease with distance from the replication origin (***Figure 1A***) as also observed by ChIP-seq (***Minnen et al., 2016***) and ChIP-chip (***Breier and Grossman, 2007***).

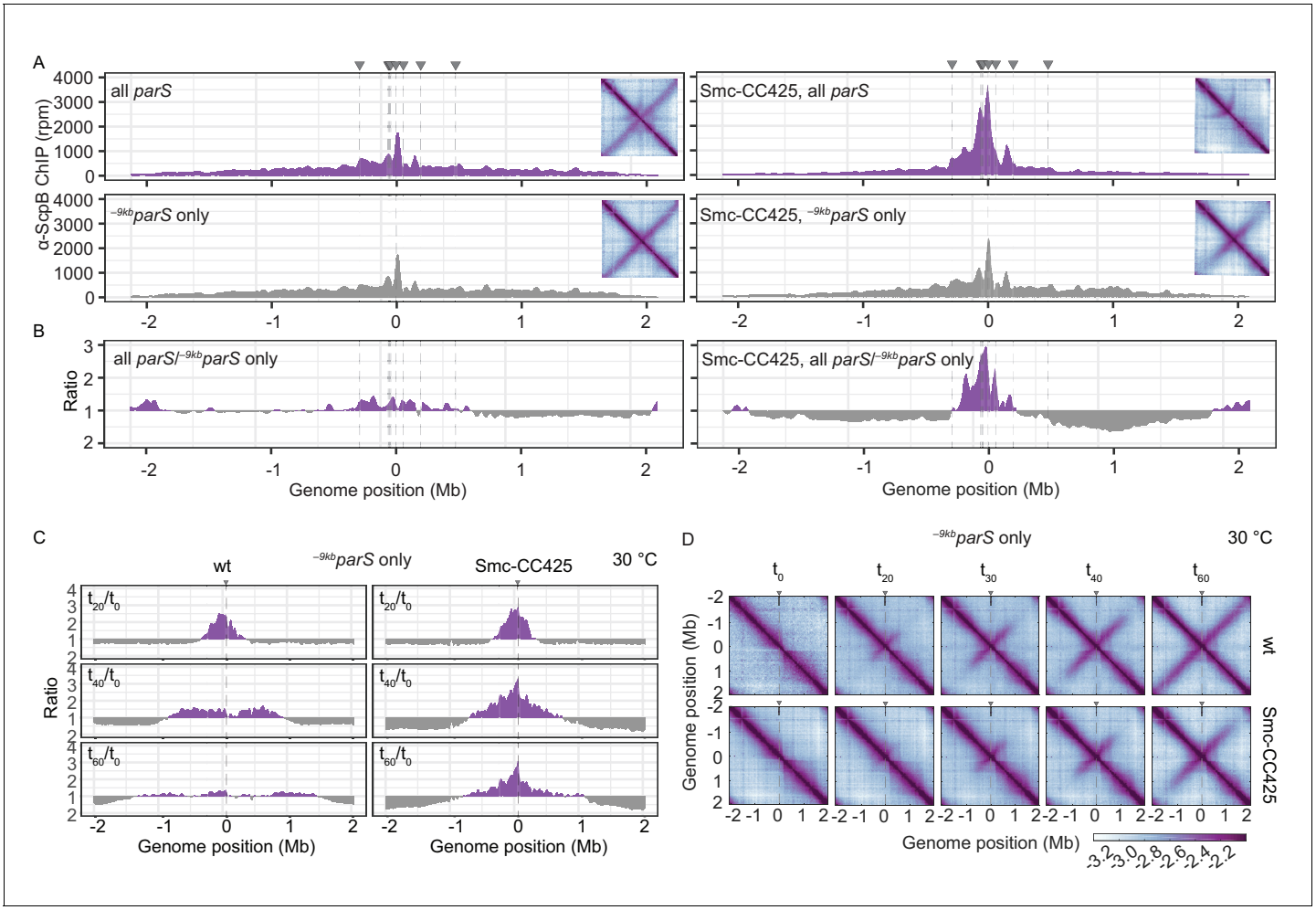

Figure 2. Modified Smc proteins hyper-accumulate in the replication origin region. (**A**) Read count distribution for chromatin immunoprecipitation coupled to deep sequencing (ChIP-seq) using α-ScpB serum. Left panel: strains carrying wild-type Smc with wild-type *parS* sites (top) or single $^{-9kb}parS_{opt}$ (*parS-359*) site (bottom). Removal of *parS* sites results in a slightly reduced enrichment in the origin region and in turn modestly increased signal mainly on the right arm of the chromosome (supposedly due to the presence of the weak $^{+1058kb}parS$ site; *parS-90*). Right panel: strains carrying Smc with elongated coiled coil (Smc-CC425) with wild-type *parS* sites (top) or single $^{-9kb}parS_{opt}$ (*parS-359*) site (bottom). Insets depict corresponding 3C-seq contact maps. All ChIP-seq profiles presented in this study are divided into 1 kb bins and have the replication origin placed in the middle. Dashed lines indicate the position of *parS* sites. (**B**) Ratio plots of ChIP-seq read counts for wild-type and elongated Smc (Smc-CC425) shown in (**A**). For each bin, normalized read counts for single $^{-9kb}parS_{opt}$ were compared with respective wild-type *parS* values. If the mutant/wild-type ratio was > 1, it was plotted above the genome position axis (in violet colors). If the mutant/wild-type ratio was < 1, the inverse ratio was plotted below the axis (in gray colors). (**C**) ChIP-seq time-course experiments using α-ScpB serum for strains carrying wild-type (left panel) or elongated Smc (Smc-CC425, right panel). These strains harbor a single loading site, $^{-9kb}parS_{opt}$ (*parS-359*), and a theophylline-inducible *parB* gene. Ratios plots of read counts for a given time point (t_x) versus t_0 are shown. For each bin, normalized read counts were compared with respective t_0 value and the higher value was divided by the lower. If the ratio t_x/t_0 was > 1, it was plotted above the genome position axis (in violet colors). If the ratio t_0/t_x was > 1, the inverse ratio was plotted below the axis (in gray colors). (**D**) Normalized 3C-seq contact maps for the time course experiments with strains carrying wild-type (top panel) or elongated Smc (Smc-CC425, bottom panel), corresponding to (**C**).

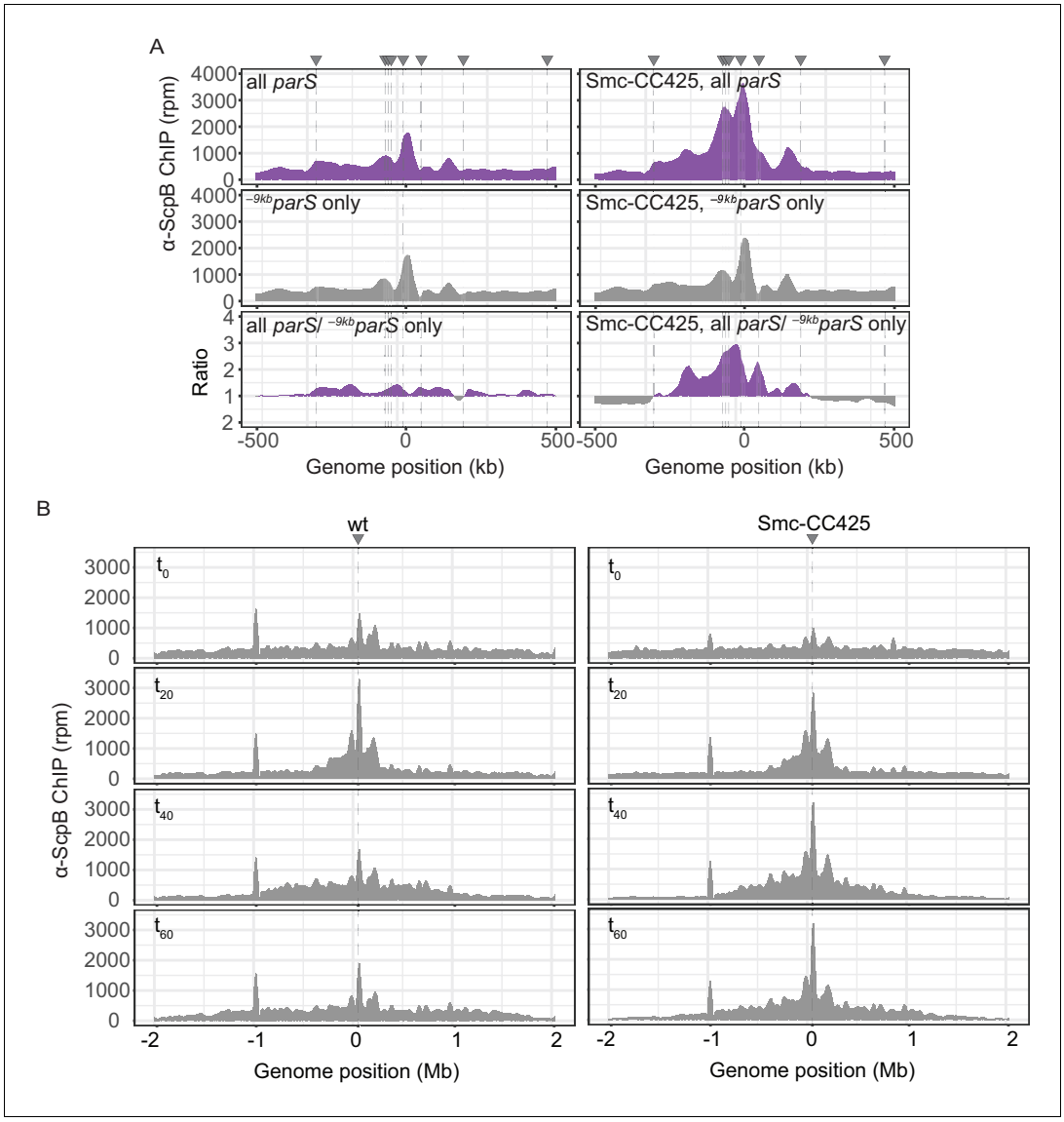

Figure 2—figure supplement 1. Enrichment of Smc and Smc-CC425 in the replication origin region. (**A**) Closeup view of ChIP-seq profiles shown in ***Figure 1A, B***. Lines indicate *parS* site positions. (**B**) Read count distribution for chromatin immunoprecipitation coupled to deep sequencing (ChIP-seq) using α-ScpB serum for the ratio plots presented in ***Figure 2C***. Left panel: strain carrying wild-type Smc. Right panel: strain carrying Smc-CC425. Both strains harbor a single loading site, $^{-9kb}parS_{opt}$ (*parS-359*), and a parB gene under the control of a theophylline-riboswitch. Triangles indicate positions of *parS* sites. Dashed lines denote the presence of a *parS* site in a given strain.

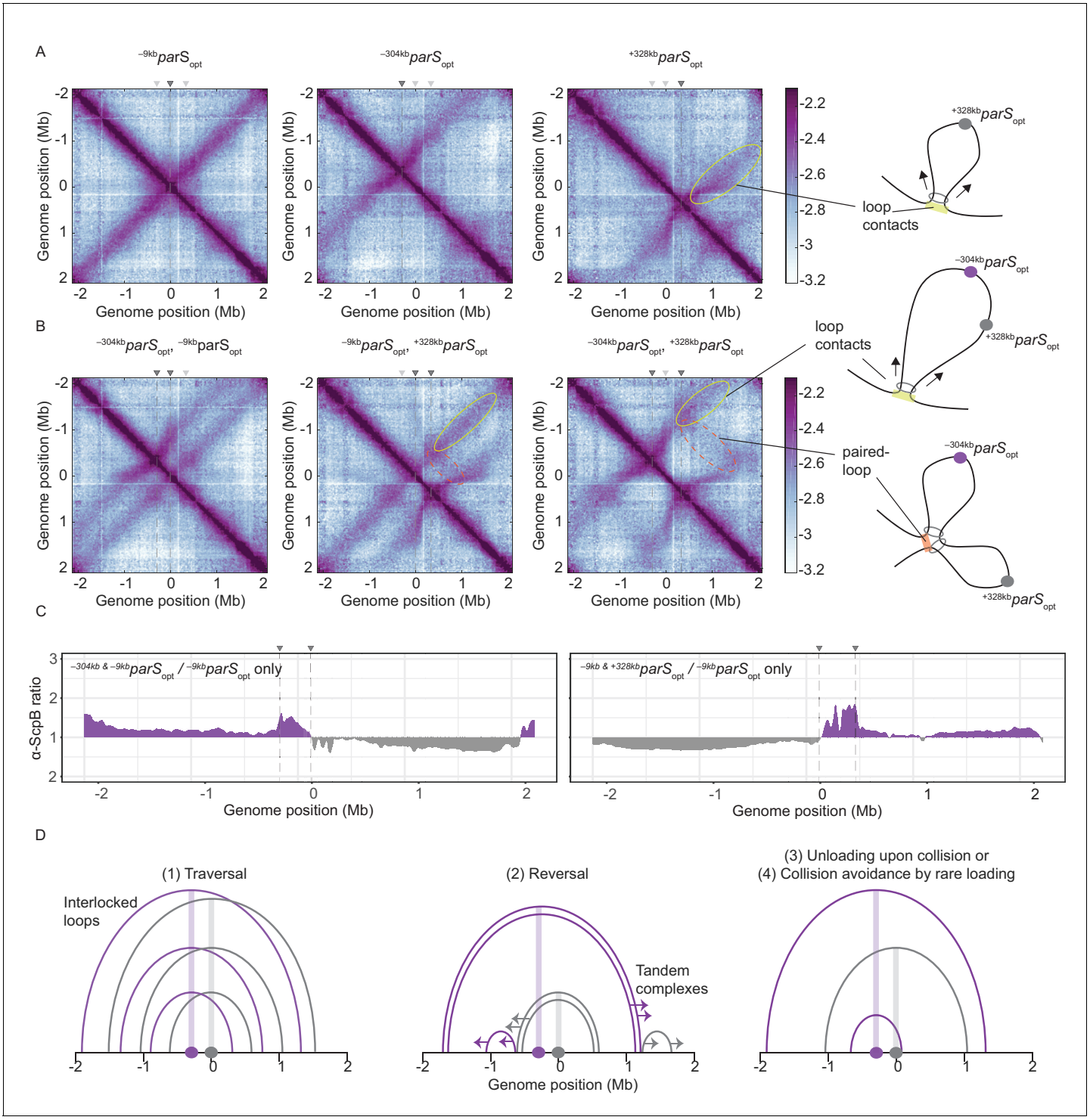

Figure 3. Overlapping chromosome arm alignment patterns for wild-type Smc. (**A**) Normalized 3C-seq contact maps for strains with a single $parS_{opt}$ site at −9 kb, −304 kb, or +328 kb. Dark gray triangles above the contact maps indicate the presence of active *parS* sites. Light gray triangles for reference are *parS* sites absent in the given experiment. Schemes depict a 'loop contact' that emerges by bidirectional translocation of a Smc unit from a single loading site (yellow), here $^{+328kb}parS_{opt}$. (**B**) Normalized 3C-seq contact maps for strains with two $parS_{opt}$ sites spaced by ~300 kb (left and middle) or ~600 kb (right). Schemes interpreting interactions in the contact maps: loop contacts (in yellow colors) and 'paired-loop contacts' that we presume to emerge by collision of two convergently translocating Smc units loaded at opposite *parS* sites (in orange colors). (**C**) Ratio plots for ChIP-seq read counts for a strain with two *parS* sites (left panel: $^{-304kb}parS_{opt}$ and $^{-9kb}parS_{opt}$; right panel: $^{-9kb}parS_{opt}$ and $^{+328kb}parS_{opt}$) and a control strain with a single *parS* site ($^{-9kb}parS_{opt}$). Representation as in ***Figure 2B***. (**D**) Schemes depicting possible scenarios for long-distance contacts emerging by

Figure 3 continued on next page

Figure 3 continued

bidirectional Smc translocation with collision avoidance and collision resolution: Smc traversal (1), reversal (2), unloading upon collision (3), or low Smc flux (4).

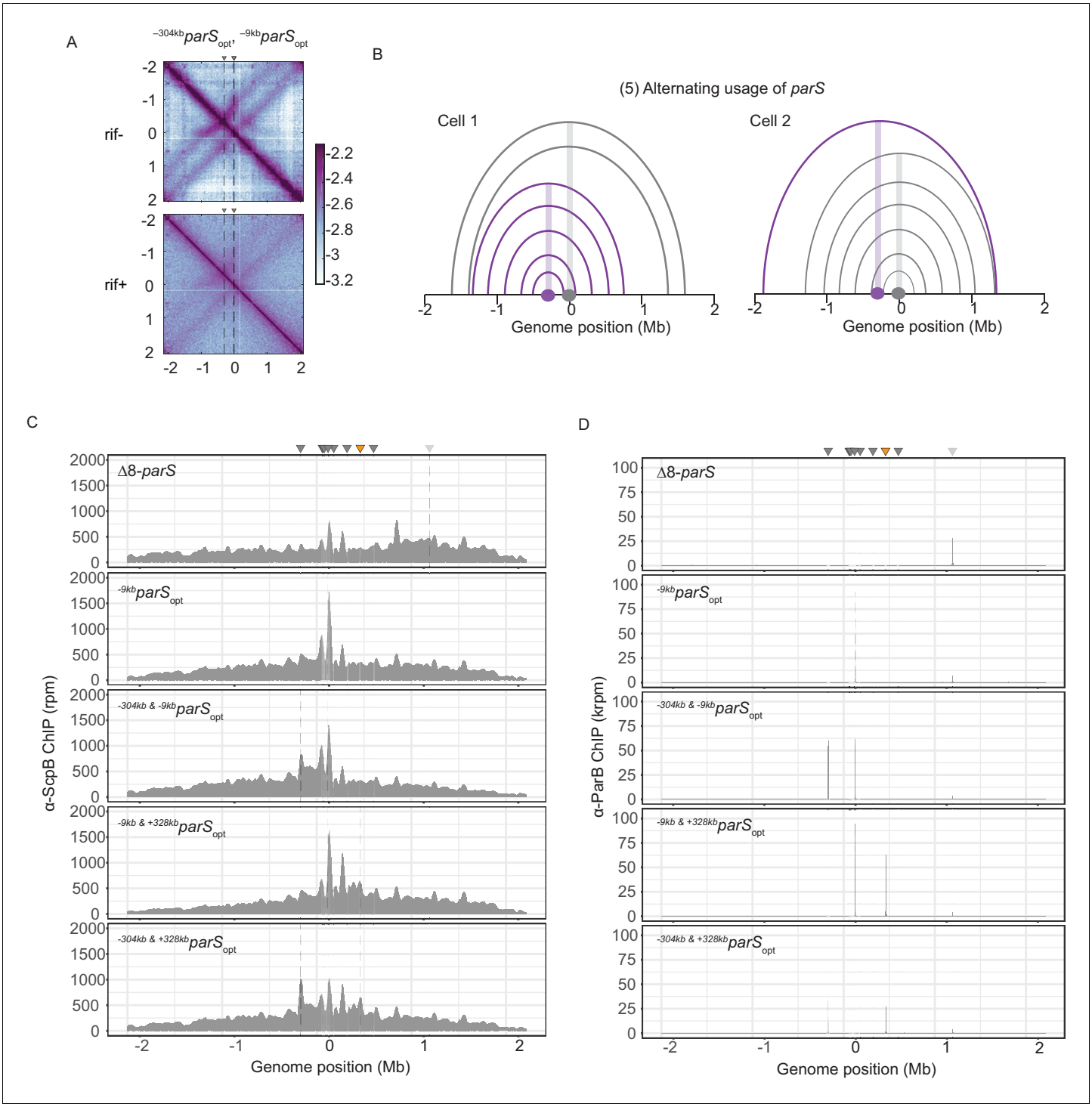

Figure 3—figure supplement 1. Wild-type Smc protein generates overlapping chromosome folding patterns. (**A**) RNAP inhibition experiment using rifampicin. Normalized 3C-seq contact maps for strains with two $parS_{opt}$ sites spaced by ~300 kb (mock treatment control 'rif-', top panel) (rif treatment 'rif+', bottom panel). (**B**) Schemes depicting possible scenario for collision avoidance and collision resolution: exclusive usage of a single *parS* site by SMC complexes as a consequence of temporary inactivation of remaining *parS* sites. (**C**) Read count distribution for chromatin immunoprecipitation coupled to deep sequencing (ChIP-seq) using α-ScpB serum for a strain with eight *parS* sites deleted, single $parS_{opt}$ at −9 kb, two *parS* sites at −304 kb and −9 kb, −9 kb and +328 kb or −304 kb and +328 kb. Represented as in ***Figure 2—figure supplement 1B***. (**D**) Read count distribution for chromatin immunoprecipitation coupled to deep sequencing (ChIP-seq) using α-ParB serum as in ***Figure 3—figure supplement 1C***.

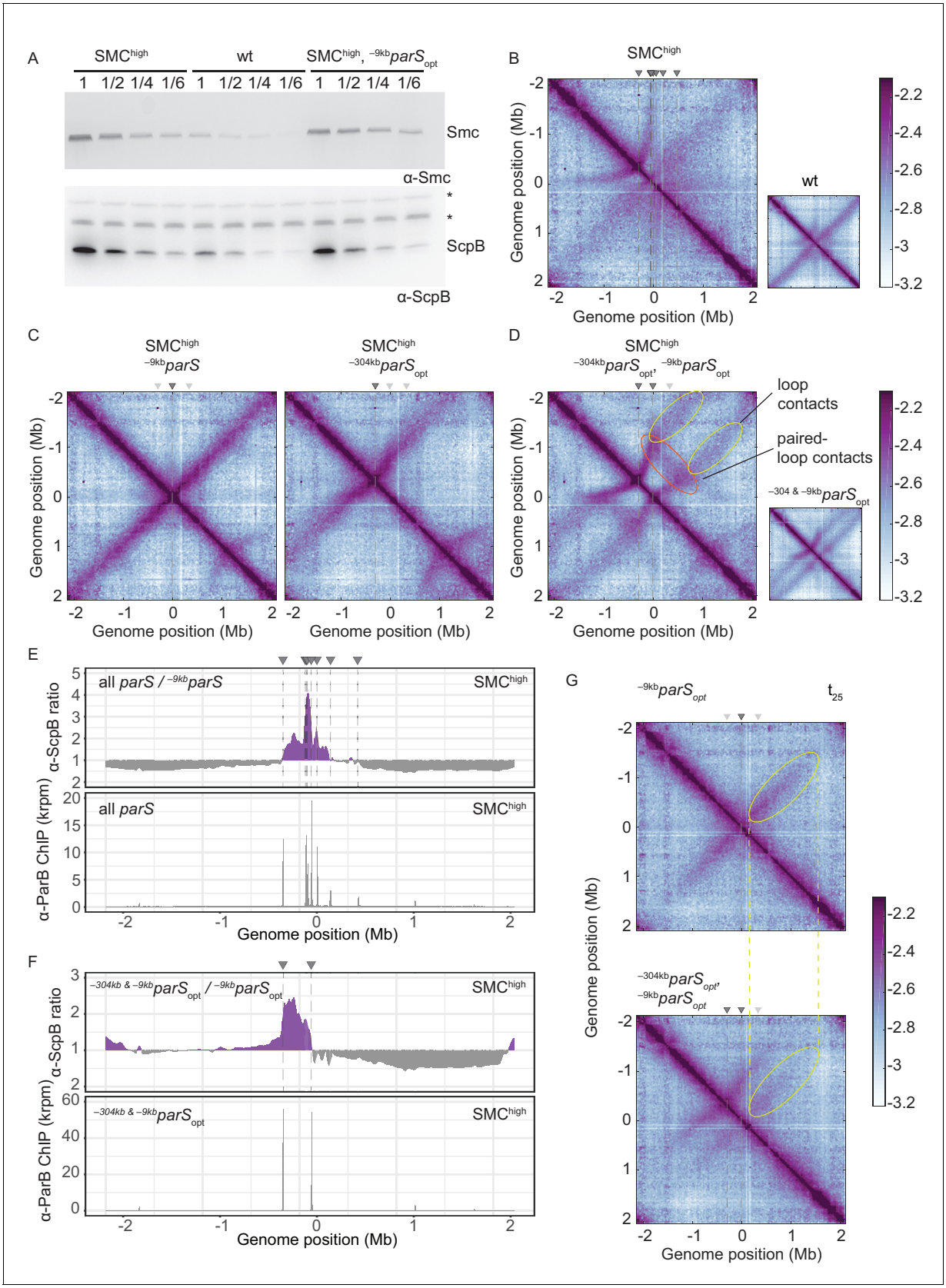

Figure 4. Increasing the cellular pool of Smc hampers chromosome organization. (**A**) Immunoblotting using α-Smc (top panel) and α-ScpB serum (bottom panel). SMC^{high} denotes strains with extra genes for Smc-ScpAB. Protein extracts of wild-type or SMC^{high} strains (harboring all *parS* sites or

Figure 4 continued on next page

Figure 4 continued

single *parS* site) were serially diluted with extracts from Δ*smc* or Δ*scpB* strains as indicated (see Materials and methods). * indicates unspecific bands generated by the α-ScpB serum. (**B**) Normalized 3C-seq contact map for SMC^{high} strain with all *parS* sites present. Inset shows 3C-seq contact map of a strain with wild-type protein levels (also displayed in ***Figure 1C***) for direct comparison. (**C**) Normalized 3C-seq contact maps for SMC^{high} strains with $parS_{opt}$ at −9 kb only or at −304 kb only. (**D**) Normalized 3C-seq contact map for SMC^{high} strain with $parS_{opt}$ at positions: −9 kb and −304 kb. As in (**B**), with inset displaying respective control strain with normal Smc expression levels (also shown in ***Figure 3B***). (**E**) Ratio plots for ChIP-seq read counts comparing SMC^{high} strains with all *parS* sites and a single *parS* site ($^{-9kb}parS_{opt}$). Representation as in ***Figure 2B*** (top panel). Read count for α-ParB ChIP-seq in SMC^{high} strain (bottom panel). (**F**) As in (**E**) involving a SMC^{high} strain with two *parS* sites ($^{-304kb}parS_{opt}$ and $^{-9kb}parS_{opt}$) instead of all *parS* sites. (**G**) Normalized 3C-seq contact maps for time point t_{25} after IPTG-induced ParB expression with a single $parS_{opt}$ site (top panel) or two $parS_{opt}$ sites (at −9 kb and −304 kb) (bottom panel). Ellipsoids (in yellow colors) mark the position of contacts stemming from loop extrusion originating at $^{-9kb}parS_{opt}$.

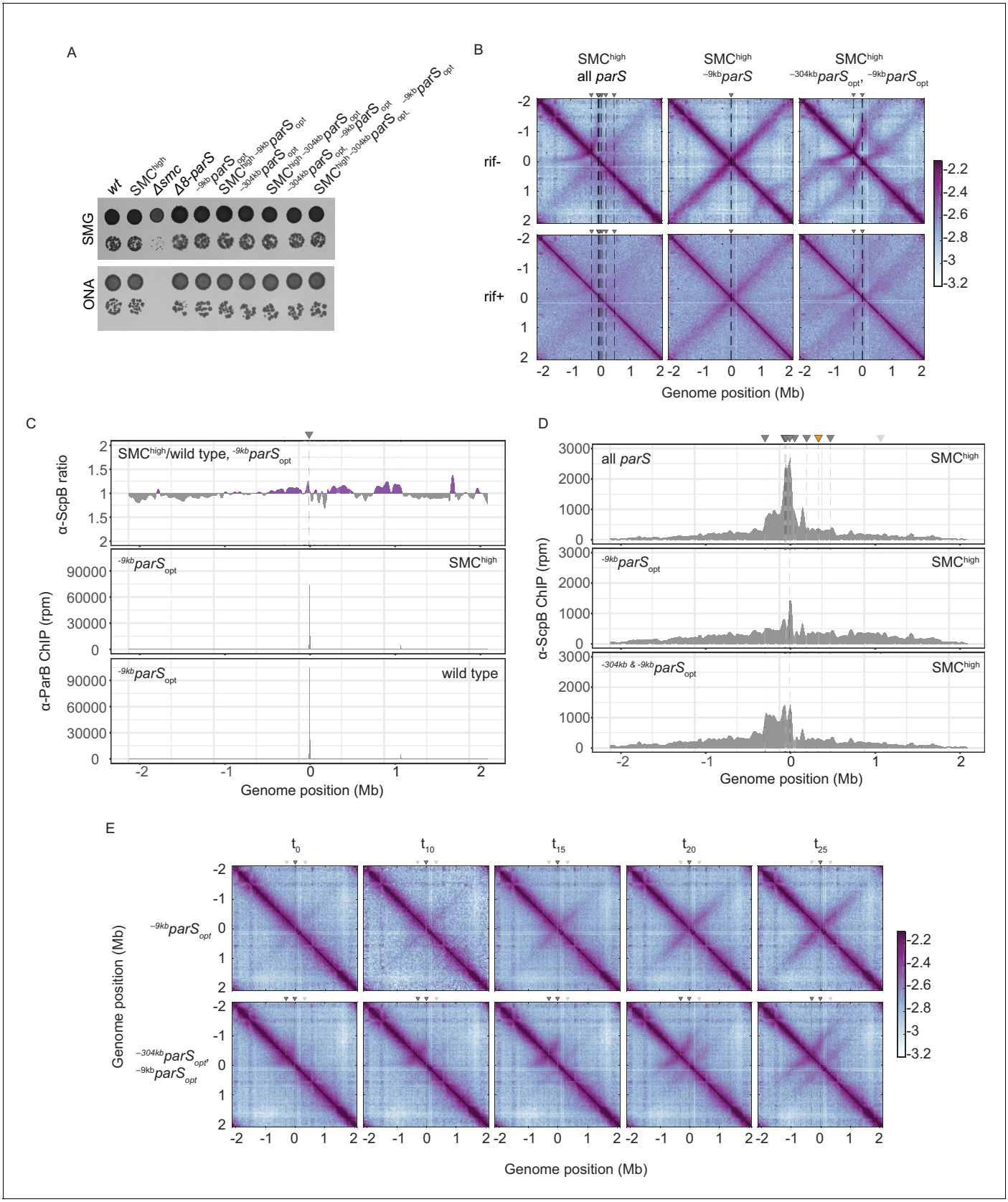

Figure 4—figure supplement 1. Synchronized loading of SMC hampers chromosome organization. (**A**) Spotting assay comparing strains with extra Smc-ScpAB genes to wild-type strains with normal or altered *parS* site distribution. Prepared as described in ***Figure 1B***. (**B**) RNAP inhibition experiment

Figure 4—figure supplement 1 continued on next page

Figure 4—figure supplement 1 continued

using rifampicin. Normalized 3C-seq contact maps for SMC^{high} strains with all, single $^{-9kb}parS_{opt}$, or two $parS_{opt}$ sites spaced by ~300 kb (mock treatment controls 'rif-', top panels) (rif treatment, 'rif+', bottom panels). (**C**) Ratio plots for ChIP-seq read counts comparing SMC^{high} strain and wild-type levels of Smc with a single *parS* site ($^{-9kb}parS_{opt}$). Representation as in ***Figure 2B*** (top panel). Read count for α-ParB ChIP-seq in the SMC^{high} and wild-type Smc strains (middle and bottom panels, respectively). (**D**) α-ScpB ChIP-seq read counts for SMC^{high} strains with all *parS* sites present (top panel), single $parS_{opt}$ at position −9 kb (middle panel), and two *parS* sites at positions −304 kb and −9 kb (bottom panel). Represented as in ***Figure 3—figure supplement 1C***. (**E**) Normalized 3C-seq contact maps for time-course experiments for strains with a single loading site $parS_{opt}$ (at −9 kb, top panels) or two $parS_{opt}$ (at −304 kb and −9 kb, bottom panels) and IPTG-inducible ParB.